



Supplement of

Multidecadal ozone trends in China and implications for human health and crop yields: a hybrid approach combining a chemical transport model and machine learning

Jia Mao et al.

Correspondence to: Amos P. K. Tai (amostai@cuhk.edu.hk)

The copyright of individual parts of the supplement might differ from the article licence.

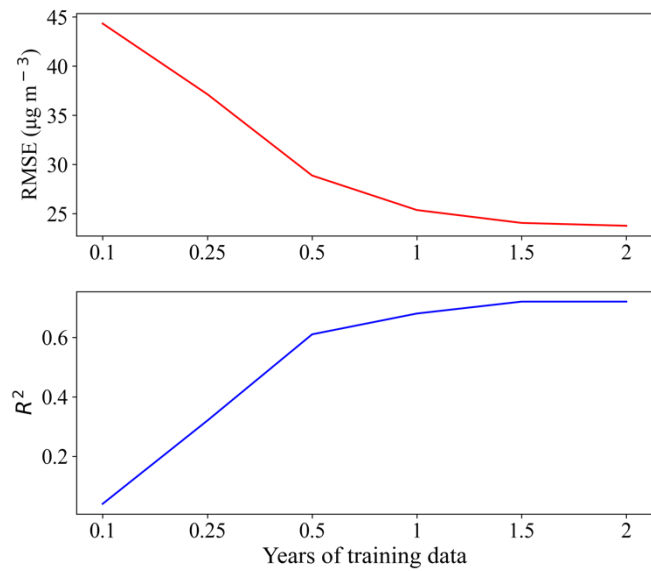


Figure S1. Testing statistics with increasing length of training data for MDA8-O₃.

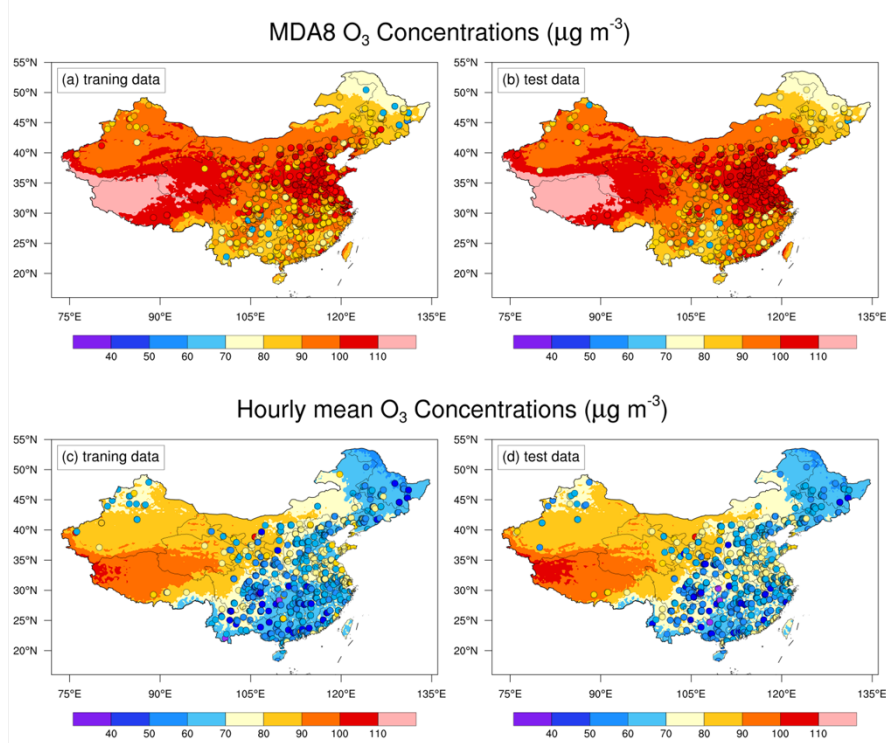


Figure S2. The spatial distribution of O₃ observations (dots) and hybrid model predictions (shaded): (a) MDA8-O₃ concentrations of training data; (b) MDA8-O₃ concentrations of test data; (c) hourly O₃ concentrations of training data; and (d) hourly O₃ concentrations of test data.

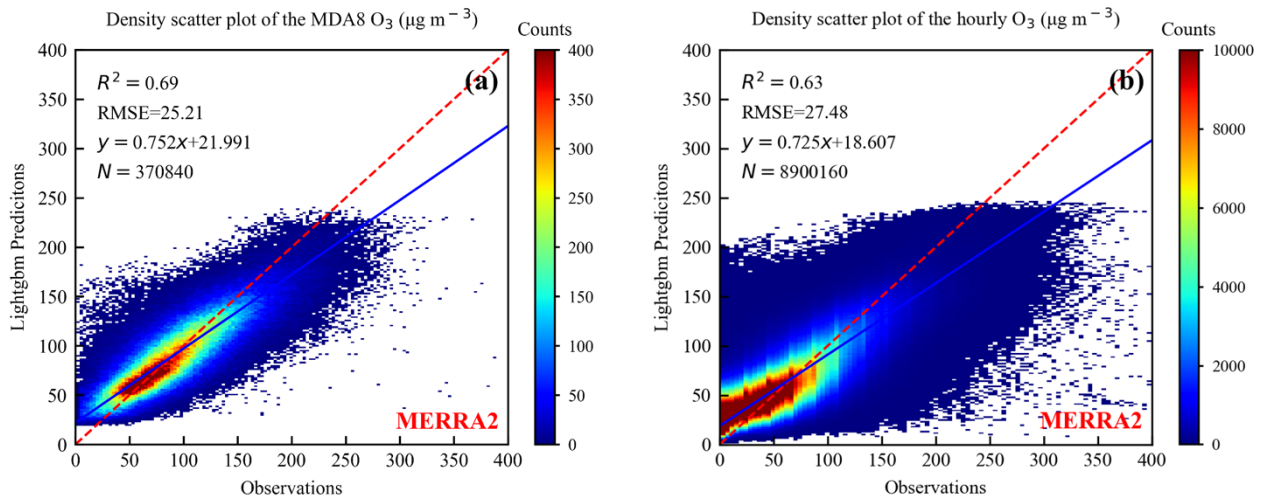


Figure S3. Density scatter plots and linear regression statistics of LightGBM bias-corrected O₃ predictions using MERRA2 meteorology vs. observation for 2018: (a) MDA8-O₃ vs. observations; and (b) hourly O₃ vs. observations. The model results are sampled at the same locations. The dashed red line indicates the 1:1 line, and the solid blue line indicates the line of best fit using orthogonal regression. The R^2 is the coefficient of determination, RMSE is the root-mean-square error, and N is the number of data points. The X and Y axis represents the O₃ observations and predictions, respectively.

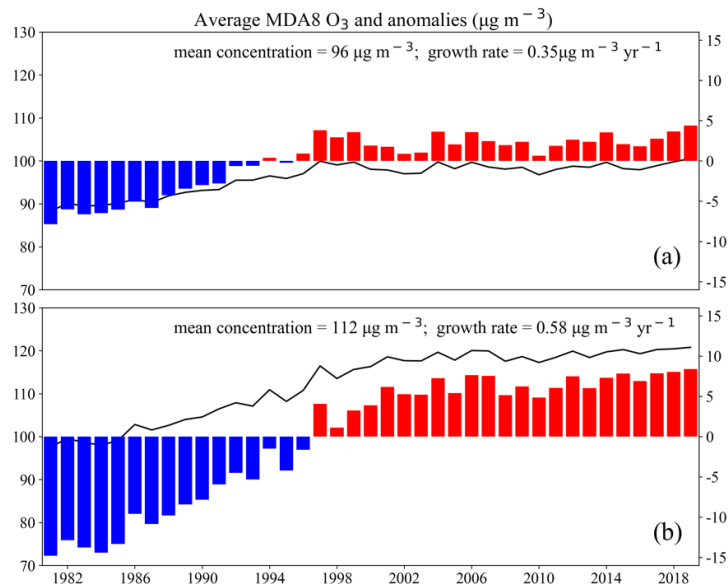


Figure S4. The GEOS-Chem-simulated MDA8-O₃ predictions (black line; left y axis) and corresponding anomalies (colored bar; right y axis) from 1981 to 2019: (a) annual mean; and (b) warm-season mean (May-September). Observed trends (growth rate) are obtained by ordinary linear regression on mean values of MDA8-O₃. The anomalies are defined as annual mean minus the multi-decadal average over 1981-2019.

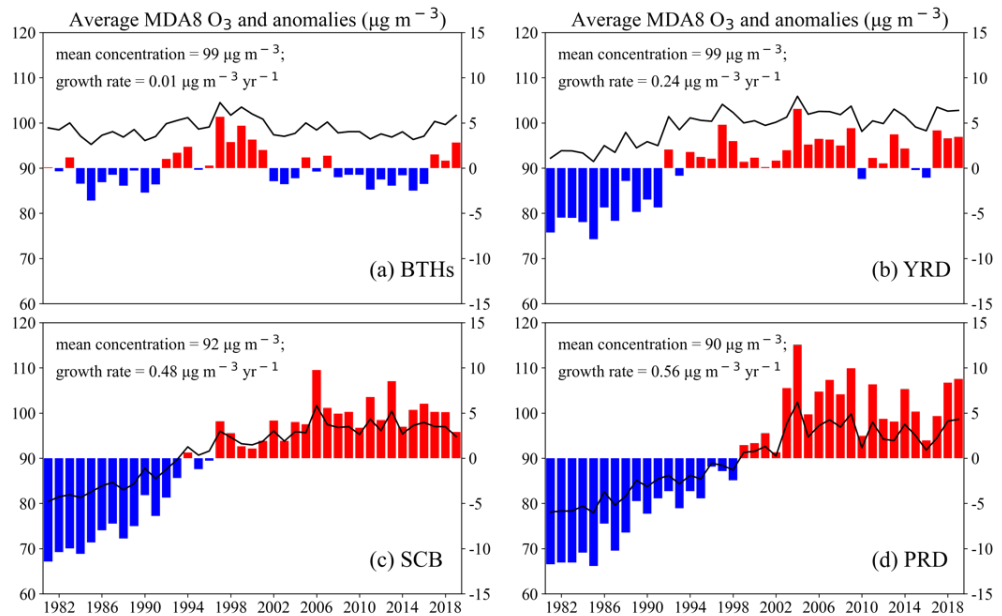


Figure S5. The annual averaged MDA8-O₃ concentrations of bias-corrected predictions (black line; left y axis) and corresponding anomalies (colored bar; right y axis) from 1981 to 2019: (a) BTHs; (b) YRD; (c) SCB; and (d) PRD. Observed trends (growth rate) are obtained by ordinary linear regression on mean values of MDA8-O₃.

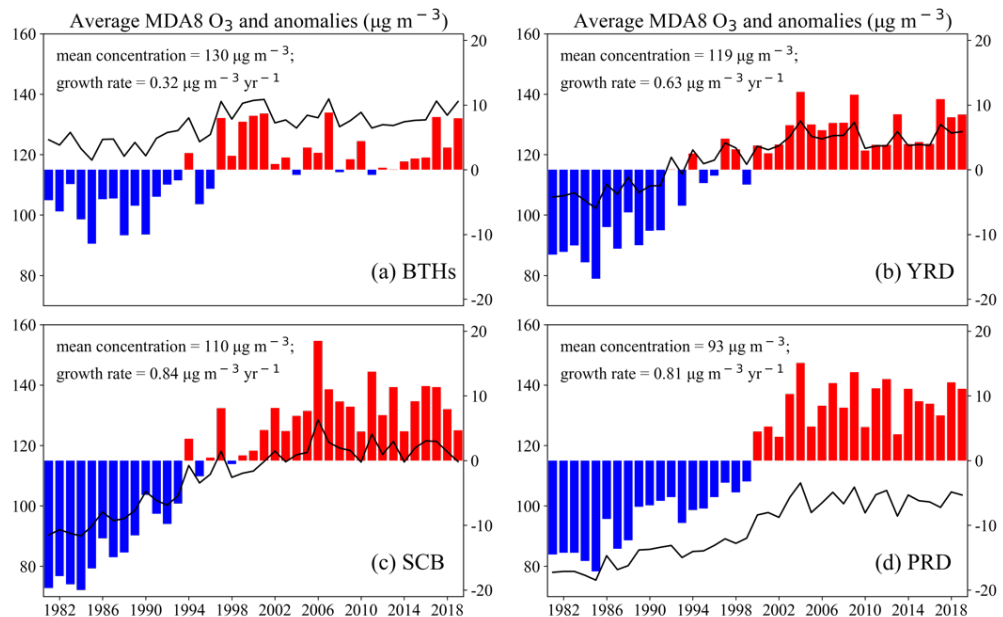


Figure S6. The same as Figure S5, but for warm-season averaged MDA8-O₃ concentrations.

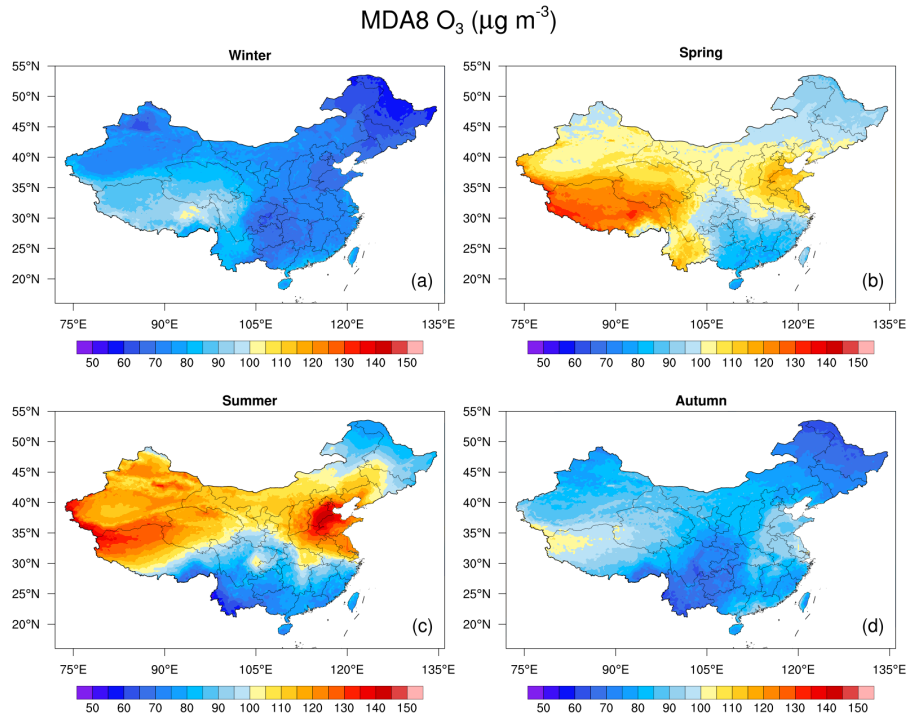


Figure S7. Spatial distribution of the bias-corrected MDA8-O₃ predictions ($\mu\text{g m}^{-3}$) from 1981–1990: (a) winter; (b) spring; (c) summer; and (d) fall.

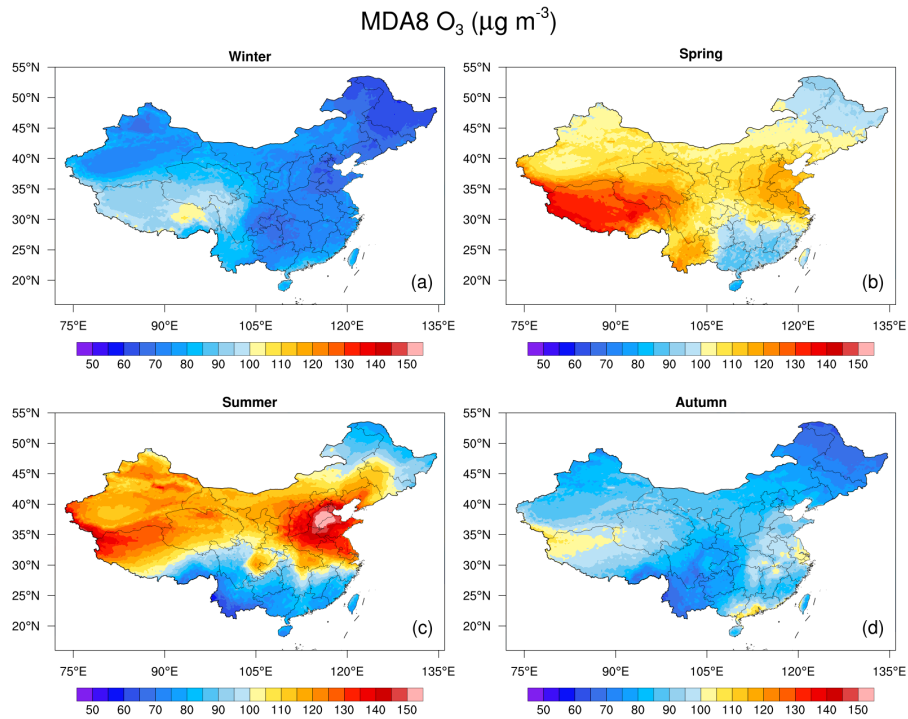


Figure S8. Same as Fig. S7 but for the period of 1991–2000.

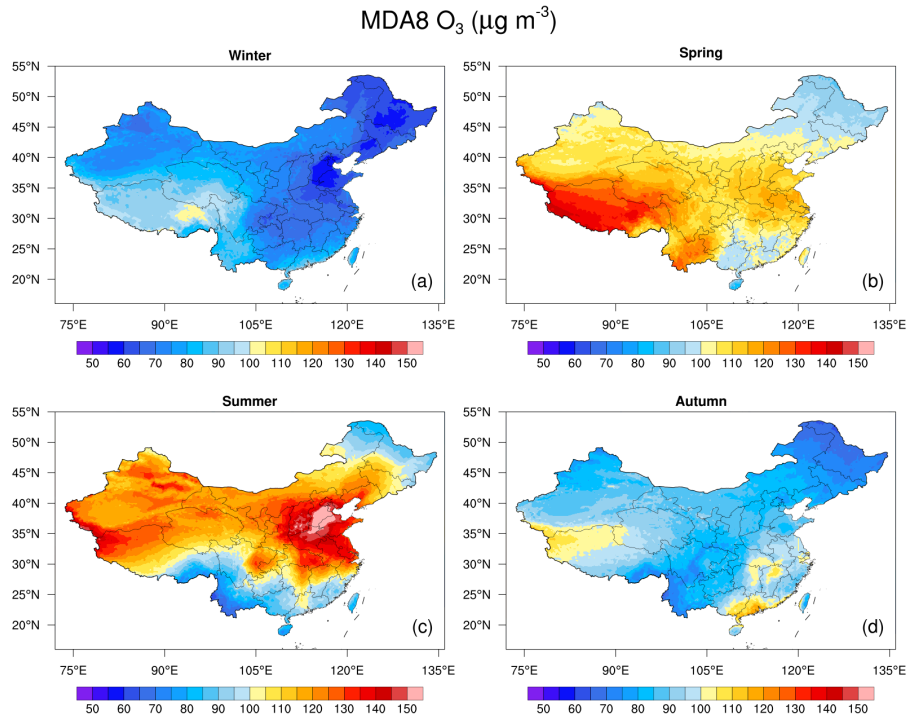


Figure S9. Same as Fig. S7 but for the period of 2001–2010.

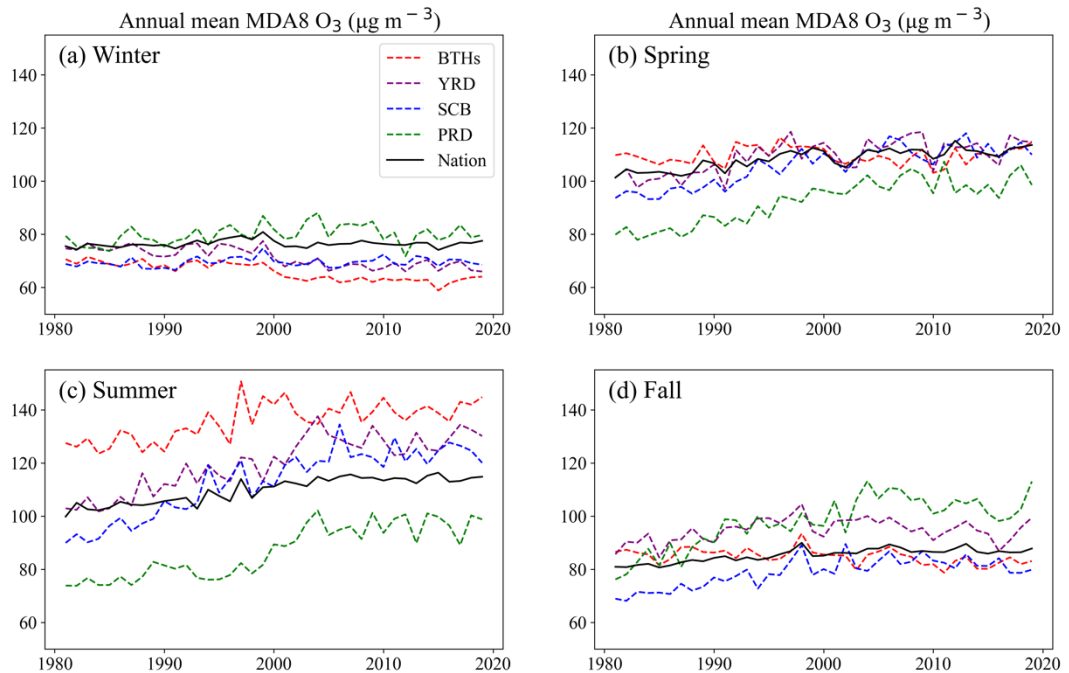


Figure S10. The seasonal averaged bias-corrected MDA8-O₃ concentrations in different regions from 1981 to 2019: (a) winter; (b) spring; (c) summer; and (d) fall.

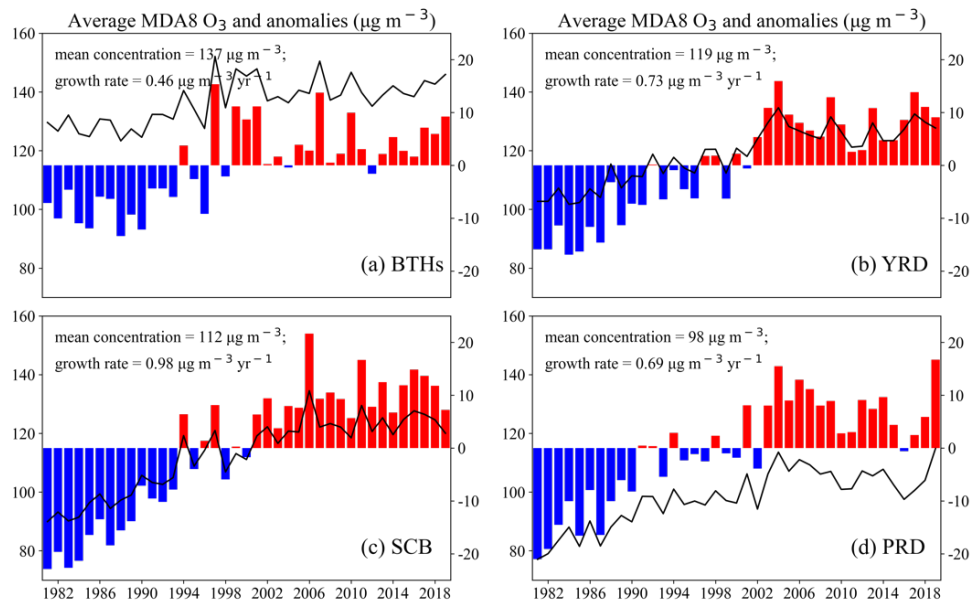


Figure S11. The same as Figure S5, but for summer averaged MDA8-O₃ concentrations in BTHs, YRD and SCB, and fall averaged MDA8-O₃ concentrations in PRD.

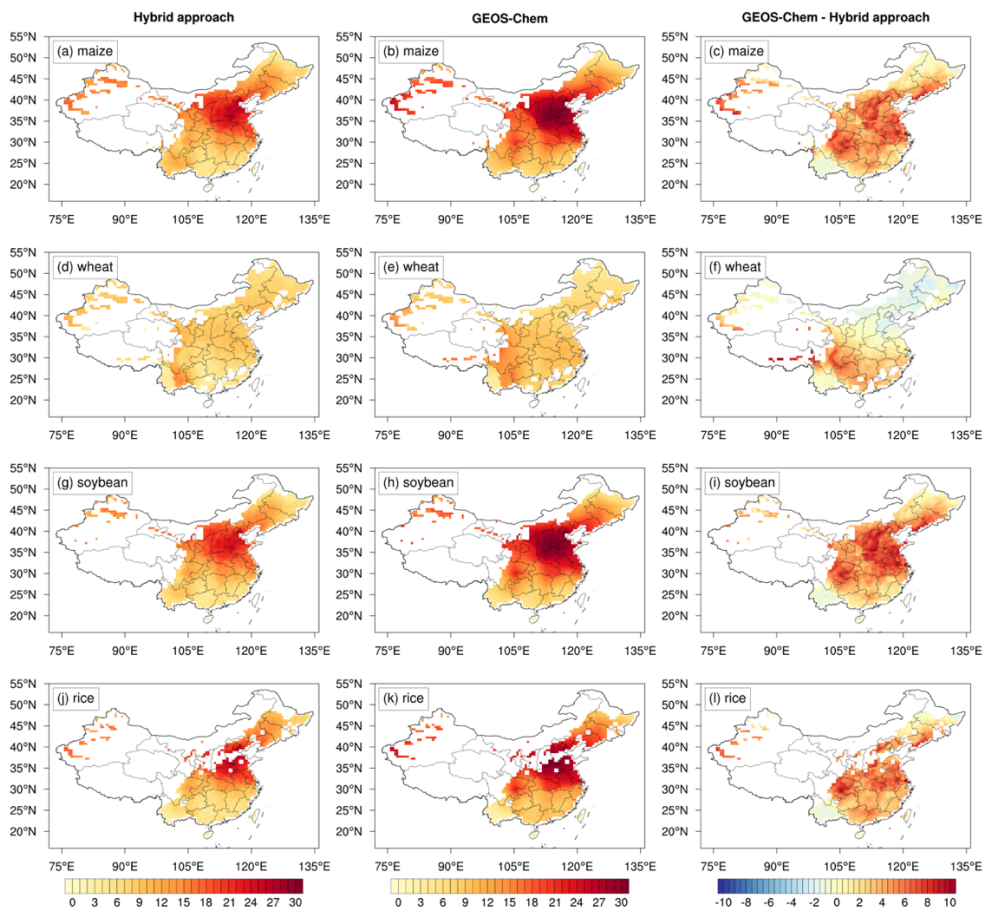


Figure S12. Spatial distribution of annual average AOT40 for four staple crops during the growing season. The estimated AOT40 using bias-corrected O₃: (a) maize; (d) wheat; (g) soybean; and (j) rice. The estimated AOT40

using GEOS-Chem-simulated O₃: (b) maize; (e) wheat; (h) soybean; and (k) rice. The differences in estimated AOT40 between GEOS-Chem-simulated and bias-corrected O₃: (c) maize; (f) wheat; (i) soybean; and (l) rice. The GEOS-Chem-simulated O₃ were regressed to 0.5°×0.5° for comparison with bias-corrected O₃.

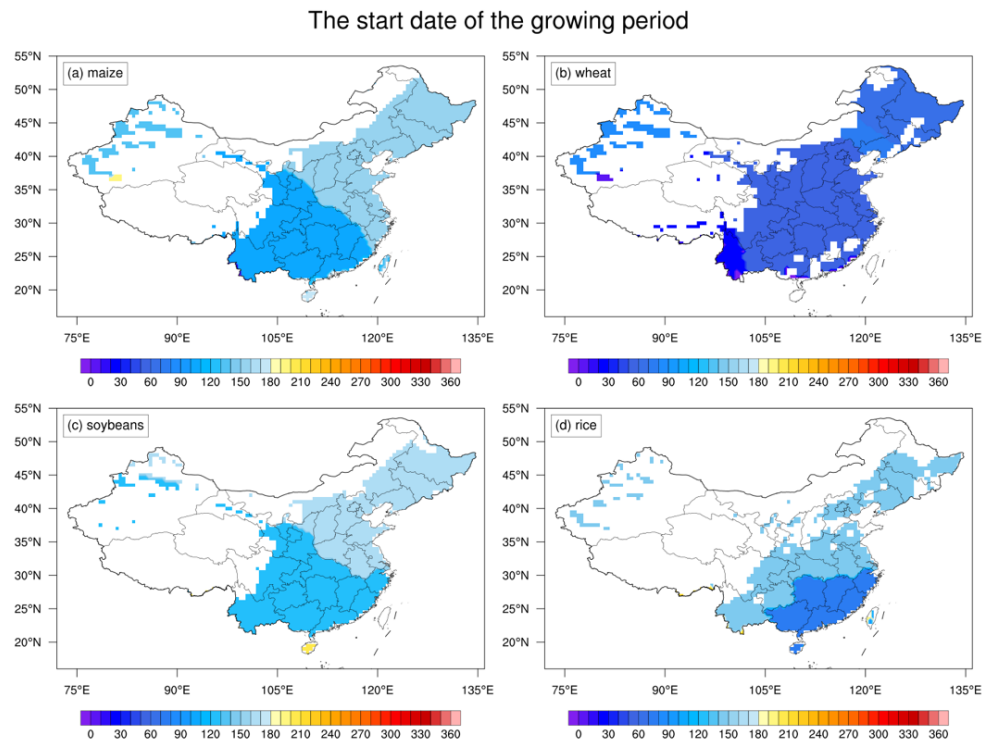


Figure S13. The start of the growing period for crops: (a) maize; (b) wheat; (c) soybean; and (d) rice. The growing period are defined as the 90 days prior to the start of the harvesting period according to the crop calendar.

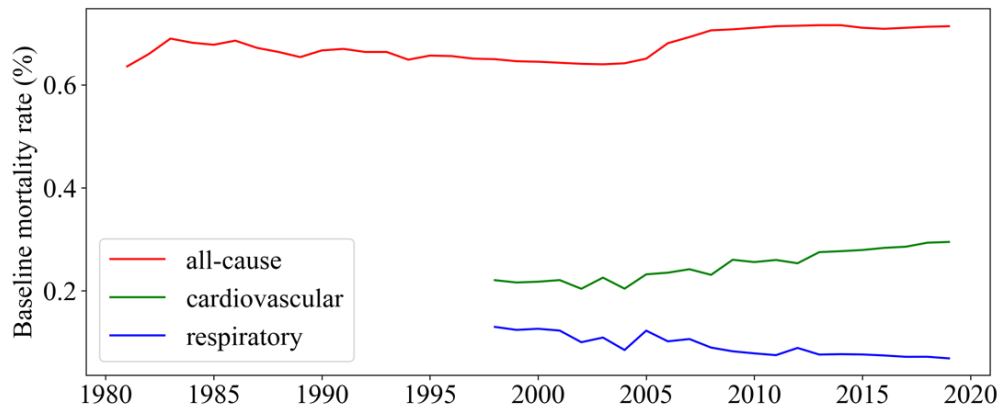


Figure S14. Annual baseline mortality rate (%) for particular disease: (a) all-cause disease; (b) cardiovascular disease; and (c) respiratory disease.

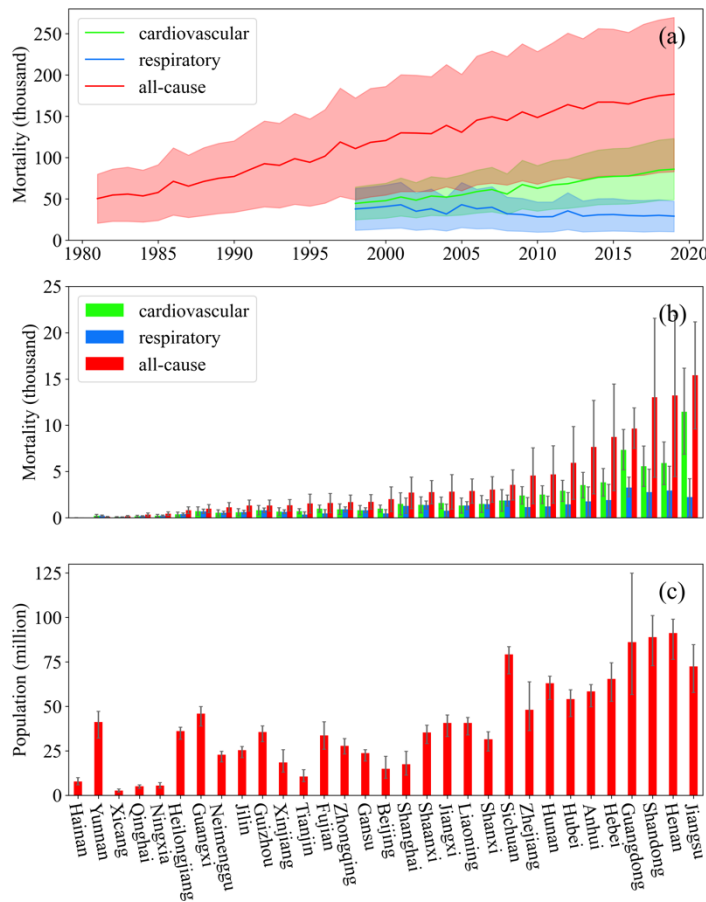


Figure S15. (a) Annual premature mortality (thousand) for different diseases over the past decades; (b) annual mean province-based mortality (thousand) attributed to different health endpoints; and (c) annual mean province-based population (million). The mortality is calculated using the GEOS-Chem-simulated O₃.

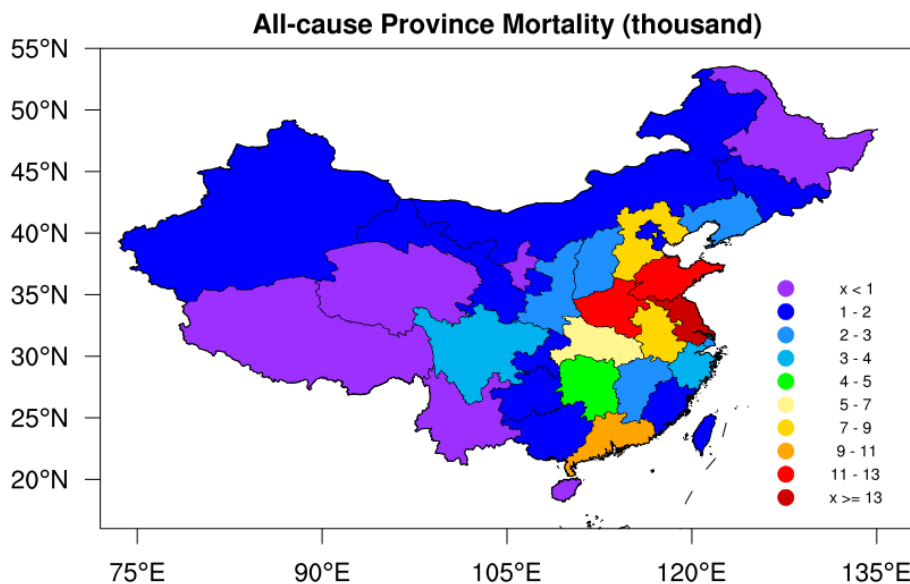


Figure S16. Provincial annual premature mortality (thousand) for all-cause diseases from 1981 to 2019.

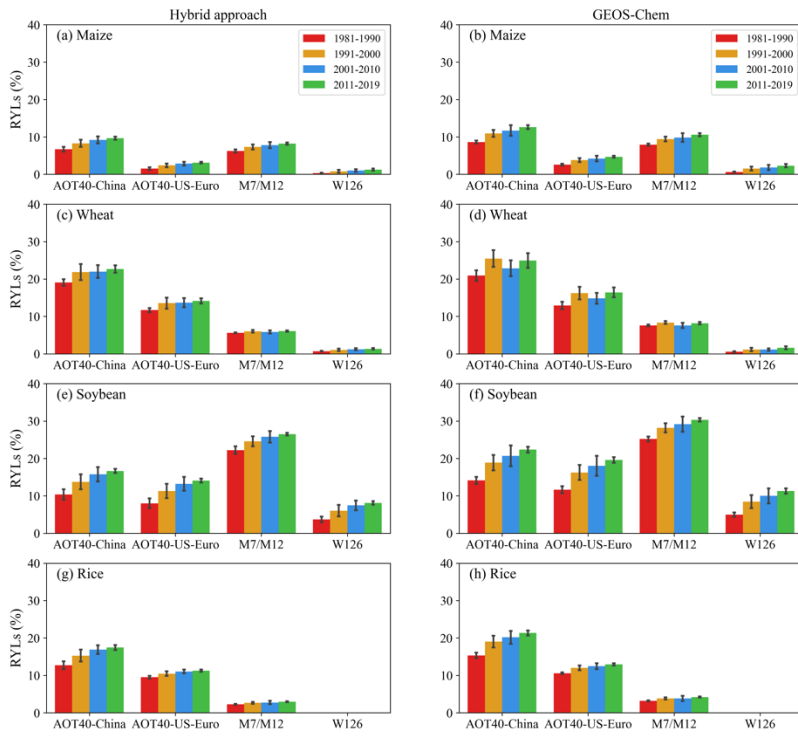


Figure S17. The estimated decadal mean relative yield losses (RYLs) of four staple crops using different metrics and dose-yield relationships from 1981–2019. The estimated RYLs using bias-corrected O₃: (a) maize; (c) wheat; (e) soybean; and (g) rice. The estimated RYLs using GEOS-Chem-simulated O₃: (b) maize; (d) wheat; (f) soybean; and (h) rice. The error bar represents the standard deviation. The dose-yield relationships of AOT40-US-Euro for four crops are derived from (Mills et al., 2007), M7 for rice and wheat are from (Adams et al., 1989), M12 for soybean and maize are from (Lesser et al., 1990), and W126 for maize, wheat and soybean are from (Tai et al., 2021), respectively.

Table S1 Statistical relationships between relative yields (RYs) and AOT40. RY is defined as the ratio of O₃-affected yield to the unaffected yield at zero O₃ exposure.

Crop	Dose-yield relationship	References
Maize	$RY = 1 - S[AOT40 + (40 - x) * 1.08 - (20.22 - 0.01264x^2) / (1 + 0.207 AOT40 - 0.0001293x^2 AOT40)] / [1 - S (22.98 - 1.08x + 0.01264x^2)],$ $S = 0.0068$ and $x = 40.0$	(Feng et al., 2022)
Wheat	$RY = 1 - S[AOT40 + (40 - x) * 1.08 - (20.22 - 0.01264x^2) / (1 + 0.207 AOT40 - 0.0001293x^2 AOT40)] / [1 - S (22.98 - 1.08x + 0.01264x^2)],$ $S = 0.0161$ and $x = 26.5$	(Feng et al., 2022)
Soybean	$RY = 1 - 0.012AOT40$	(Zhang et al., 2017)
Rice	$RY = 1 - S[AOT40 + (40 - x) * 1.08 - (20.22 - 0.01264x^2) / (1 + 0.207 AOT40 - 0.0001293x^2 AOT40)] / [1 - S (22.98 - 1.08x + 0.01264x^2)],$ $S = 0.0071$ and $x = 19.4$	(Feng et al., 2022)

Table S2 Exposure-response coefficients for the short-term health impacts of O₃.

Health outcomes	Coefficients β	95% CI	Study region/year	Referenced paper
All-cause	4.5E-04	1.6E-04 – 7.3E-04	Shanghai (2001–04)	(Zhang et al., 2006)
	5.5E-04	3.4E-04 – 7.6E-04	Jiangsu (2013–14)	(Chen et al., 2017)
	8.1E-04	6.3E-04 – 1.00E-03	PRD (2006–08)	(Tao et al., 2011)
	3.6E-04	1.2E-04 – 6.0E-04	East China (2005–30)	(Madaniyazi et al., 2016)
	2.4E-04	1.3E-04 – 3.5E-04	Nationwide (2013–15)	(Yin et al., 2017)
Cardiovascular	5.3E-04	1.0E-04 – 9.6E-04	Shanghai (2001–04)	(Zhang et al., 2006)
	9.8E-04	5.8E-04 – 1.4E-03	Jiangsu (2013–14)	(Chen et al., 2017)
	1.01E-03	7.1E-04 – 1.32E-03	PRD (2006–08)	(Tao et al., 2011)
	3.8E-04	2.3E-04 – 5.3E-04	East China (2005–30)	(Madaniyazi et al., 2016)
	2.7E-04	1.0E-04 – 4.4E-04	Nationwide (2013–15)	(Yin et al., 2017)
Respiratory	3.5E-04	-4.0E-04 – 1.09E-03	Shanghai (2001–04)	(Zhang et al., 2006)
	1.3E-03	8.9E-04 – 1.76E-03	PRD (2006–08)	(Tao et al., 2011)
	5.1E-04	3.0E-05 – 9.8E-04	East China (2005–30)	(Madaniyazi et al., 2016)
	7.3E-04	4.9E-04 – 9.7E-04	Nationwide	(Shang et al., 2013)

Table S3 The information of the candidate variables used for training.

Symbols	Units	Description	Source
GEOS_O ₃	ppb	GEOS-Chem-simulated O ₃	GEOS-Chem output
Lat	°	Latitude of site/grid	

Lon	°	Longitude of site/grid	
Hourly_O ₃	µg m ⁻³	Hourly mean O ₃ concentration	Calculated from GEOS_O ₃
Monthly_O ₃	µg m ⁻³	Monthly mean O ₃ concentration	Calculated from GEOS_O ₃
Albedo		Surface albedo	ERA5
SSRD	J m ⁻²	Downward surface solar radiation	ERA5
SP	Pa	Surface pressure	ERA5
T2M	K	Air temperature at 2m	ERA5
RH_1000hPa	%	Relative humidity at 1000 hPa	ERA5
RH_850hPa	%	Relative humidity at 850 hPa	ERA5
U10	m s ⁻¹	U component of wind at 10 m	ERA5
V10	m s ⁻¹	V component of wind at 10 m	ERA5
U_1000hPa	m s ⁻¹	U component of wind at 1000 hPa	ERA5
V_1000hPa	m s ⁻¹	U component of wind at 1000 hPa	ERA5
U_850hPa	m s ⁻¹	V component of wind at 850 hPa	ERA5
V_850hPa	m s ⁻¹	V component of wind at 850 hPa	ERA5
Omega_1000hPa	Pa s ⁻¹	Vertical velocity at 1000 hPa	ERA5
Omega_850hPa	Pa s ⁻¹	Vertical velocity at 850 hPa	ERA5
Elevation	m	Elevation of site/grid	RESDC
LU		Land use type of site/grid	RESDC

Table S4 Seasonal averaged MDA8-O₃ concentrations (µg m⁻³) in each region from 1981 to 2019. The differences are GEOS-Chem minus Hybrid approach.

Seasons	Region	Hybrid approach	GEOS-Chem	Differences
Winter	BTHs	65 ± 4	63 ± 7	-2 ± 3
	YRD	73 ± 3	72 ± 7	-2 ± 4
	SCB	69 ± 2	79 ± 2	10 ± 1
	PRD	81 ± 4	87 ± 3	6 ± 2
	Nation	73 ± 2	76 ± 3	3 ± 2
Spring	BTHs	109 ± 3	102 ± 4	-7 ± 3
	YRD	109 ± 6	110 ± 5	1 ± 3
	SCB	106 ± 7	112 ± 8	7 ± 2
	PRD	93 ± 9	93 ± 11	6 ± 3
	Nation	106 ± 4	105 ± 4	-1 ± 1
Summer	BTHs	137 ± 8	142 ± 7	5 ± 2
	YRD	119 ± 10	125 ± 11	6 ± 4
	SCB	113 ± 12	120 ± 14	7 ± 3
	PRD	88 ± 10	87 ± 15	-1 ± 5
	Nation	111 ± 7	114 ± 9	3 ± 2
Fall	BTHs	83 ± 3	83 ± 5	-1 ± 2
	YRD	95 ± 4	103 ± 3	6 ± 2
	SCB	79 ± 5	95 ± 7	17 ± 3

PRD	98 ± 10	101 ± 12	3 ± 4
Nation	86 ± 3	92 ± 4	6 ± 1

References

Adams, R. M., Glycer, J. D., Johnson, S. L., and McCarl, B. A.: A Reassessment of the Economic Effects of Ozone on U.S. Agriculture, JAPCA, 39, 960-968, <https://doi.org/10.1080/08940630.1989.10466583>, 1989.

Chen, K., Zhou, L., Chen, X., Bi, J., and Kinney, P. L.: Acute effect of ozone exposure on daily mortality in seven cities of Jiangsu Province, China: No clear evidence for threshold, Environmental Research, 155, 235-241, <https://doi.org/10.1016/j.envres.2017.02.009>, 2017.

Feng, Z., Xu, Y., Kobayashi, K., Dai, L., Zhang, T., Agathokleous, E., Calatayud, V., Paoletti, E., Mukherjee, A., Agrawal, M., Park, R. J., Oak, Y. J., and Yue, X.: Ozone pollution threatens the production of major staple crops in East Asia, Nature Food, 3, 47-56, <https://doi.org/10.1038/s43016-021-00422-6>, 2022.

Lesser, V. M., Rawlings, J. O., Spruill, S. E., and Somerville, M. C.: Ozone Effects on Agricultural Crops: Statistical Methodologies and Estimated Dose-Response Relationships, Crop Science, 30, cropsci1990.0011183X003000010033x, <https://doi.org/10.2135/cropsci1990.0011183X003000010033x>, 1990.

Madaniyazi, L., Nagashima, T., Guo, Y., Pan, X., and Tong, S.: Projecting ozone-related mortality in East China, Environment International, 92-93, 165-172, <https://doi.org/10.1016/j.envint.2016.03.040>, 2016.

Mills, G., Buse, A., Gimeno, B., Bermejo, V., Holland, M., Emberson, L., and Pleijel, H.: A synthesis of AOT40-based response functions and critical levels of ozone for agricultural and horticultural crops, Atmospheric Environment, 41, 2630-2643, <https://doi.org/10.1016/j.atmosenv.2006.11.016>, 2007.

Shang, Y., Sun, Z., Cao, J., Wang, X., Zhong, L., Bi, X., Li, H., Liu, W., Zhu, T., and Huang, W.: Systematic review of Chinese studies of short-term exposure to air pollution and daily mortality, Environment International, 54, 100-111, <https://doi.org/10.1016/j.envint.2013.01.010>, 2013.

Tai, A. P. K., Sadiq, M., Pang, J. Y. S., Yung, D. H. Y., and Feng, Z.: Impacts of Surface Ozone Pollution on Global Crop Yields: Comparing Different Ozone Exposure Metrics and Incorporating Co-effects of CO₂, Frontiers in Sustainable Food Systems, 5, <https://doi.org/10.3389/fsufs.2021.534616>, 2021.

Tao, Y., Zhong, L., Huang, X., Lu, S.-E., Li, Y., Dai, L., Zhang, Y., Zhu, T., and Huang, W.: Acute mortality effects of carbon monoxide in the Pearl River Delta of China, Science of The Total Environment, 410-411, 34-40, <https://doi.org/10.1016/j.scitotenv.2011.09.004>, 2011.

Yin, P., Chen, R., Wang, L., Meng, X., Liu, C., Niu, Y., Lin, Z., Liu, Y., Liu, J., Qi, J., You, J., Zhou, M., and Kan, H.: Ambient Ozone Pollution and Daily Mortality: A Nationwide Study in 272 Chinese Cities, Environ Health Perspect, 125, 117006, <https://doi.org/10.1289/EHP1849>, 2017.

Zhang, W., Feng, Z., Wang, X., Liu, X., and Hu, E.: Quantification of ozone exposure- and stomatal uptake-yield response relationships for soybean in Northeast China, Science of The Total Environment, 599-600, 710-720, <https://doi.org/10.1016/j.scitotenv.2017.04.231>, 2017.

Zhang, Y., Huang, W., London Stephanie, J., Song, G., Chen, G., Jiang, L., Zhao, N., Chen, B., and Kan, H.: Ozone and Daily Mortality in Shanghai, China, Environmental Health Perspectives, 114, 1227-1232, <https://doi.org/10.1289/ehp.9014>, 2006.